

# Discovery of subdiffusion problem with noisy data via deep learning

Xingjian Xu · Minghua Chen

Received: date / Accepted: date

**Abstract** Data-driven discovery of partial differential equations (PDEs) from observed data in machine learning has been developed by embedding the discovery problem. Recently, the discovery of traditional ODEs dynamics using linear multistep methods in deep learning have been discussed in [Racheal and Du, *SIAM J. Numer. Anal.* 59 (2021) 429-455; Du et al. arXiv:2103.11488]. We extend this framework to the data-driven discovery of the time-fractional PDEs, which can effectively characterize the ubiquitous power-law phenomena. In this paper, identifying source function of subdiffusion with noisy data using  $L_1$  approximation in deep neural network is presented. In particular, two types of networks for improving the generalization of the subdiffusion problem are designed with noisy data. The numerical experiments are given to illustrate the availability using deep learning. To the best of our knowledge, this is the first topic on the discovery of subdiffusion in deep learning with noisy data.

**Keywords** Deep learning, discovery of subdiffusion, noisy data

## 1 Introduction

Deep learning has been extended to many different practical fields, including image analysis, natural language processing, system recognizing etc [10]. There are already some important progress for numerically solving the ODEs and PDEs systems in deep learning. For example, variational methods [9, 11, 13, 8], Galerkin methods [26, 2], random particle method [31], different operators method [16], linear multistep method [7]. Based on the the neural networks, the data-driven discovery of differential equations has been proposed in [29, 23, 25, 22, 21, 7] including the space-fractional differential equations [12]. In particular, the discovery of traditional ODEs dynamics using linear multistep methods in deep learning have been discussed in [7, 14] and [29]. Identifying source function from observed data is a meaningful and challenge topic for the time-dependent PDEs.

---

X. Xu · M. Chen (✉)

School of Mathematics and Statistics, Gansu Key Laboratory of Applied Mathematics and Complex Systems, Lanzhou University, Lanzhou 730000, P.R. China  
email:chenmh@lzu.edu.cn;

Over the few decades, fractional models have been attracted wide interest since it can effectively characterize the ubiquitous power-law phenomena with noise data [6, 15], which are applied in underground environment problems, transport in turbulent plasma, bacterial motion transport, etc. [19]. In this work, we study the discovery of the following subdiffusion in deep learning with noise data, whose prototype is [15, 18, 30], for  $0 < \alpha \leq 1$ ,

$$\begin{cases} {}_0^C D_t^\alpha u(x, t) + Au(x, t) = f(x, t) := \bar{f}(x, t) + \text{perturbation (noise)}, \\ u(0, t) = 0, \quad u(l, t) = 0, \quad t \in (0, T], \\ u(x, 0) = g(x), \quad x \in [0, l] \end{cases} \quad (1.1)$$

with  $A$  a positive definite, selfadjoint, linear Laplacian operator. The Caputo fractional derivative [20] is defined by

$${}_0^C D_t^\alpha u(x, t) = \begin{cases} \frac{1}{\Gamma(1-\alpha)} \int_0^t \frac{\partial u(x, \eta)}{\partial \eta} (t-\eta)^{-\alpha} d\eta, & 0 < \alpha < 1, \\ \frac{\partial u(x, t)}{\partial t}, & \alpha = 1, \end{cases} \quad (1.2)$$

and  $f$  is a given forcing term  $\bar{f}$  with noise data. In practice,  $f$  is not completely known and is disturbed around some known quantity  $\bar{f}$ , i.e.,

$$f(x, t) = \bar{f}(x, t) + \text{perturbation (noise)}.$$

Here  $\bar{f}$  is deterministic and is usually known while no exact behavior exists of the perturbation (noise) term. The uncertainty (lack of information) about  $f$  (the perturbation term) is naturally represented as a stochastic quantity, see [32]. In the following, we focus on the uniform noise and Gaussian noise. More general noise [32] such as white noise, Wiener process or Brownian motion (which corresponds to the stochastic fractional PDEs [15, 30]) can be similarly studied, since it can be discretized as like uniform noise form by a simple arithmetic operations [15, 18, 30].

The main contribution of this paper is to discover subdiffusion via  $L_1$  approximation in deep learning with noisy data, where we design two types neural networks to deal with the fractional order  $\alpha$ , since  $\alpha$  is a variable parameter. More concretely, we use two strategies (fixed  $\alpha$  and variable  $\alpha$ , respectively) to train network, which improves the generalization for the subdiffusion problem. The advantage of first Type is that model (4.2) can be trained for each fixed  $\alpha$ , which reduces the computational count and required storage, since it fixes  $\alpha$  as input data. Obviously, it may loss some accuracy. To recover the accuracy, second Type is complemented, which needs more computational count. It implies an interesting generalized structure by combining Type 1 and Type 2, which may keep suitable accuracy and reduces computational count.

The paper is organized as follows. In the next section, we introduce the discretization schemes for the subdiffusion problem (1.1) and its discovery of subdiffusion in Section 3. We construct the discovery of subdiffusion based on the basic deep neural network (DNN) in Section 4. The two types DNN are designed/developed for the subdiffusion model in Section 5. To show the effectiveness of the presented schemes, results of numerical experiments with noisy data are reported in Section 6. Finally, we conclude the paper with some remarks on the presented results.

## 2 Subdiffusion problem

In this section, we introduce the  $L_1$  approximation for solving the subdiffusion. Let  $t_n = nh_t$ ,  $n = 0, 1, \dots, N_t$  be a partition of the time interval  $[0, T]$  with the grid size  $\tau = T/N_t$ . Denote the mesh points  $x_m = mh_x$ ,  $m = 0, 1, \dots, N_x$  with the uniform grid size  $h_x = l/M$ ,  $\Omega = (0, l)$ .

The objective for solving the initial value problem in (1.1) is to find the approximation  $u_m^n \approx u(x_m, t_n)$  for given source function  $f(x_m, t_n)$ .

The diffusion term is approximated by a standard second-order discretization:

$$u_{xx}(x_m, t_n) \approx \delta_x^2 u_m^n := \frac{u_{m+1}^n - 2u_m^n + u_{m-1}^n}{h^2}. \quad (2.1)$$

There are several ways to discretize the Caputo fractional substantial derivative (1.2). For convenience, we use the following standard  $L_1$  scheme [3, 28, 17] with the truncation error  $\mathcal{O}(\tau^{2-\alpha})$ , namely,

$${}_0^C D_t^\alpha u(x_m, t_n) \approx D_\tau^\alpha u_m^n = \frac{1}{\Gamma(1-\alpha)} \sum_{k=0}^{n-1} \frac{u_m^{k+1} - u_m^k}{\tau} \int_{t_k}^{t_{k+1}} (t_n - s)^{-\alpha} ds = \sum_{k=0}^n \omega_{n-k}^{(\alpha)} u_m^k. \quad (2.2)$$

Here the coefficients are computed by  $\omega_0^{(\alpha)} = \frac{1}{\Gamma(2-\alpha)\tau^\alpha}$ ,  $\omega_n^{(\alpha)} = \frac{(n-1)^{1-\alpha} - n^{1-\alpha}}{\Gamma(2-\alpha)\tau^\alpha}$  and

$$\omega_{n-k}^{(\alpha)} = \frac{(k+1)^{1-\alpha} - 2k^{1-\alpha} + (k-1)^{1-\alpha}}{\Gamma(2-\alpha)\tau^\alpha}, \quad 1 \leq k \leq n-1.$$

Thus, we approximate (1.1) by the discrete problem with given  $f(x_m, t_n) = f_m^n$

$$\sum_{k=0}^n \omega_{n-k}^{(\alpha)} u_m^k - \delta_x^2 u_m^n = f_m^n. \quad (2.3)$$

*Remark 2.1* When  $0 < \alpha < 1$ , the time Caputo fractional derivative uses the information of the classical derivatives at all previous time levels (non-Markovian process). If  $\alpha = 1$ , it can be seen that by taking the limit  $\alpha \rightarrow 1$  in (1.2), which gives the following equation

$$\frac{\partial u(x, t_n)}{\partial t} = \frac{u(x, t_n) - u(x, t_{n-1})}{\tau} + \mathcal{O}(\tau).$$

## 3 Discovery of subdiffusion

The discovery of subdiffusion is essentially an inverse process of solving a subdiffusion problem (1.2). That means, suppose that only the information of  $u(x_m, t_n)$  at the pairs of the uniform grid points  $\{x_m, t_n\}$  is provided, we need to recover the source function  $f$  [14]. Assume  $u(x, t)$  and  $f(x, t)$  both are unknown in subdiffusion system (1.1) with given  $u_m^n = u(x_m, t_n)$ , the target is to approximate the close-form expression for  $f(x_m, t_n)$ . We can use the approximated source function  $f_m^n$  to rebuild the discrete relation between  $f_m^n$  and  $u_m^n$ , namely,

$$f_m^n = \sum_{k=0}^n \omega_{n-k}^{(\alpha)} u_m^k - \delta_x^2 u_m^n. \quad (3.1)$$

It should be noted that (3.1) directly follows the  $L_1$  approximation in (2.3). Different from (2.3) that evaluates  $u_m^n$  given  $f_m^n = f(x_m, t_n)$ , model (3.1) computes  $f_m^n$  from the given data  $u_m^n$ . It also indicates the discovery of subdiffusion is actually an inverse process of solving the subdiffusion problem.

## 4 Neural Network approximation

In this section, we introduce the basic deep neural network (DNN) [5,24,8,23], which will be used in discovery of subdiffusion.

### 4.1 Structure of deep neural network

As the input vector  $\mathbf{x}$ , the neural network can be denoted as

$$\hat{\phi}(\mathbf{x}; \theta) = L_M \circ \sigma \circ L_{M-1} \circ \sigma \dots \sigma \circ L_1(\mathbf{x})$$

where  $\hat{\phi}$  is a nonlinear function in the whole neural network. The integer  $M$  is number of

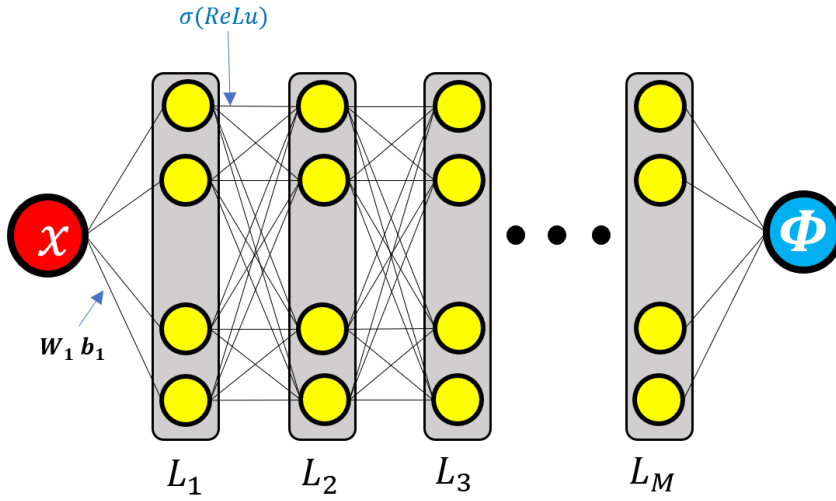


Fig. 1: Structure of deep neural network (DNN)

the layer of DNN. The  $M$ -th hidden layer has the following affine transform:

$$L_M(z) = \mathbf{W}_M z + \mathbf{b}_M, 1 \leq m \leq M \quad (4.1)$$

where  $\mathbf{W}_M, \mathbf{b}_M$  belongs to a parameter functional space  $\theta$ . The weight family  $\mathbf{W}_M \in \mathbb{R}^{p_m \times p_{m-1}}$  and collection of bias  $\mathbf{b}_M \in \mathbb{R}^{p_m}$ . The dimensional  $p_m$  is the number of neurons (width of neural network) in the  $m$ -th layer. The activation function  $\sigma$  is used as non-linear processing of information. Here we choose the ReLU function  $\sigma(t) = \max\{0, t\}$  as the activation function. All DNN structures can be presented in Figure 1.

### 4.2 Discovery of subdiffusion in deep learning

Among many different structures of approximations, it is more predominant to employ neural networks as a nonlinear approximation tool to get source function  $f(x, t)$ , which is convenient to compute and implement. So the neural network approximation is focused in this

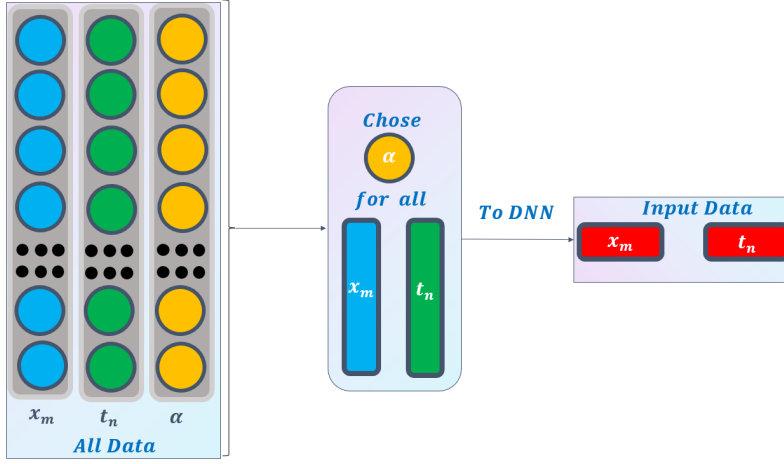


Fig. 2: The construction for Type 1 Network.

paper. Consider the neural network approximation via  $L_1$  discretization. We use  $\mathcal{N}$  as the set of all neural networks with special architecture [14]. Now we introduce a network  $\tilde{f}(\cdot) \in \mathcal{N}$  to approximate  $f(\cdot)$ . The model of neural network approximation is developed by replacing each  $f_m^n$  with  $\tilde{f}_m^n$  in (3.1)

$$\tilde{f}_m^n = \sum_{k=0}^n \omega_{n-k}^{(\alpha)} u_m^k - \delta_x^2 u_m^n. \quad (4.2)$$

Now we seek  $\tilde{f}(\cdot)$  by minimizing the residual error (4.2) under a machine learning framework in practice, namely,

$$J_h(\tilde{f}) = \min_{u \in \mathcal{N}} J_h(u) \quad (4.3)$$

with the loss function

$$J_h(u) = \frac{\sum_{m=1}^{N_x} \sum_{n=1}^{N_t} |\tilde{f}_m^n - \sum_{k=0}^n \omega_{n-k}^{(\alpha)} u_m^k + \delta_x^2 u_m^n|^2}{N_t N_x - 1}. \quad (4.4)$$

## 5 Two types of deep neural networks

It is an interesting question how we can train the discovery of subdiffusion with fractional order  $\alpha$ , since  $\alpha$  is variable parameter. Developed the structure of deep neural network in Subsection 4.1, we use two types (fixed  $\alpha$  and variable  $\alpha$ , respectively) of DNN for training the discovery of subdiffusion (4.2) in this work.

### 5.1 Type 1 of DNN: fixed $\alpha$

To train the source function  $\tilde{f}$  of subdiffusion model (4.2) by the deep neural network approximation, we design the Type 1 of DNN for the fixed  $\alpha$ , see Fig 2, which just needs  $(x_m, t_n)$  as input data.

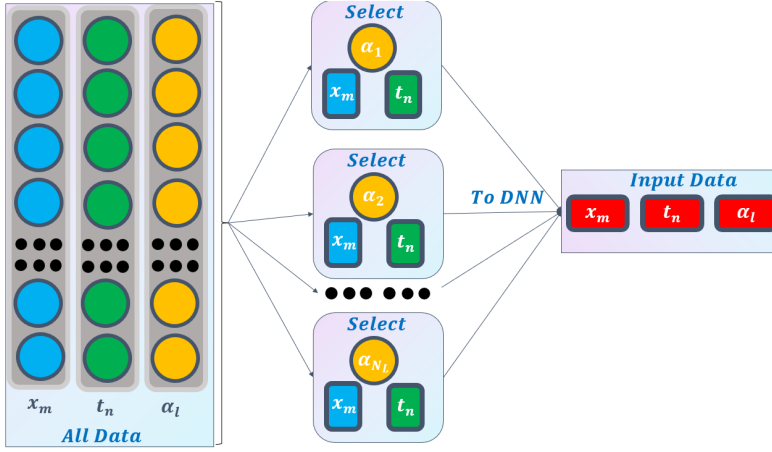


Fig. 3: The construction for Type 2 Network.

## 5.2 Type 2 of DNN: variable $\alpha$

To discover/recover the source function  $\tilde{f}$  of subdiffusion model (4.2) in DNN, we also design the Type 2 of DNN for the variable  $\alpha$ , see Fig 3, which uses  $(x_m, t_n, \alpha_l)$  as input data. Here  $\alpha$  can be chosen a sequence  $\{\alpha_l\}_{l=1}^{N_l}$ .

*Remark 5.1* The advantage of Type 1 is that model (4.2) can be trained for each fixed  $\alpha$ , which reduces the computational count and required storage, since it fixes  $\alpha$  as input data. Obviously, it may loss some accuracy. To recover the accuracy, Type 2 is complemented, which needs more computational count. Hence, there is an interesting generalized structure by combining Type 1 and Type 2, which keeps suitable accuracy and reduces computational count.

## 6 Numerical Experiments

In this section, we discover subdiffusion problem (1.1) with uniform noise and Gaussian noise in deep learning. More general noise [32] such as white noise, Wiener process or Brownian motion (which corresponds to the stochastic fractional PDEs [15,30]) can be similarly studied, since it can be discretized as like uniform noise form by a simple arithmetic operations [15, 18,30]. Several examples are provided to show the performance of subdiffusion discovery via  $L_1$  approximation in DNN by Algorithm 1.

The relative error  $\|\cdot\|_r$  is measured by

$$\|e_{\tilde{f}}\| = \frac{\left(\sum_{m=1}^{N_x} \sum_{n=1}^{N_t} |\tilde{f}_m^n - f(x_m, t_k)|^2\right)^{1/2}}{\left(\sum_{m=1}^{N_x} \sum_{n=1}^{N_t} |f(x_m, t_k)|^2\right)^{1/2}}, \quad (6.1)$$

where we actually use the well-known Frobenius norm of the  $n \times n$  matrix  $A$ , i.e.,

$$\|A\|_F = \left(\sum_{i,j=1}^n |a_{i,j}|^2\right)^{1/2}.$$

The overall setting in all experiments is summarized as following

Feature	Statement
Environment	All numerical experiments are programmed in Python 3.8, and Pytorch library for neural network are implemented.
Optimizer	Apply Adam optimization algorithm for solving minimization problem (4.4) with the learning rate $1.0 \times 10^{-2}$ .
Parameters	By fixing the epoch, the batch size is changed to derive the optimization.
Network setting	100 neurons and 10 layers with ReLU activation function in Fig. 1, and uniform distribution $\mathbf{W}_M, \mathbf{b}_M$ in (4.1) is initialized.
Two types setting	We fix the fractional order $\alpha = 0.3$ in Type 1, and choose a sequence $\alpha = \{l/10\}_{l=1}^{10}$ in Type 2.

---

### Algorithm 1 Discovery of subdiffusion in deep learning

---

**Input:** Batch size  $B_1$ ; Epoch  $I_1$ ; Learning rate  $r$ ; Size of DNN.

**Output:** Discovery  $\tilde{f}_m^n$

- 1: Generate mesh data  $x_m$  and  $t_n$  with  $h_x = h_t = 1/100$  on the interval  $[0, 1]$ .
  - 2: Calculate  $u_m^n$  with  $x_m, t_n$  and  $\alpha$  by (2.3).
  - 3: Discover  $f_m^n$  by using  $u_m^n, x_m, t_n$  in (3.1).
  - 4: Construct the training set  $\{x_m, t_n\}$  in Type 1 or  $\{x_m, t_n, \alpha\}$  in Type 2 to approximate  $f_m^n$ .
  - 5: Initialize the weights  $\mathbf{W}$  and biases  $\mathbf{b}$  in (4.1) with Normal distribution of DNN, see Fig 4.1.
  - 6: **for** iteration  $i = 1 : I_1$  in epoch **do**
  - 7:   **for** iteration  $j = 1 : B_1$  in Batch size **do**
  - 8:     Construct DNN for training set in small batch and get the output  $\tilde{f}_m^n$  in (4.2)
  - 9:     Update  $\tilde{f}_m^n$  the neural network by minimizing the loss function (4.4)
  - 10:     Update the neural network by minimizing the loss function in Fig 4.1:
  - 11:      $\mathbf{W}_{j+1} \leftarrow \mathbf{W}_j + r \times \mathbf{W}_j$
  - 12:      $\mathbf{b}_{j+1} \leftarrow \mathbf{b}_j + r \times \mathbf{b}_j$
  - 13:   **end for**
  - 14: **end for**
  - 15: Calculate the relative error  $\|\cdot\|_r$  in (6.1).
- 

#### 6.1 Numerical Experiments for discovery with uniform noise

*Example 1* Let us consider the following subdiffusion problem (1.1)

$$\begin{cases} {}_0^C D_t^\alpha u(x, t) - \Delta u = f, & x \in [0, 1], t \in [0, 1]; \\ u(x, 0) = \sqrt{x(1-x)}; \\ u(0, t) = 0, u(1, t) = 0. \end{cases}$$

Here the source function is given by

$$f(x, t) = (t + 1)^2 (1 + \chi_{(0,1/2)}(x)) + \delta$$

with

$$\chi_{(0,1/2)}(x) = \begin{cases} 1, & 0 \leq x \leq 1/2, \\ 0, & \text{otherwise.} \end{cases}$$

Here  $\delta$  is the uniform noise with 0% (clean data) 10%, 20%, 50% level for a single uniform distributed random number in the interval  $(0, 1)$ , respectively. In this experiment, we train the deep learning discovery  $\tilde{f}$  in (4.2).

### 6.1.1 Type 1 in DNN

Table 1 and Figures 4-7 show the relative error (6.1) between the source function  $f$  in Example 1 and discovery  $\tilde{f}$  in (4.2) with epoch=250 in Type 1. From Table 1, it can be found that our proposed algorithm is stable and accurate faced with different discretization sizes and noise level, which is robust even for 50% uniformly distributed noise level.

Table 1: **The relative error  $\|e_{\tilde{f}}\|_r$  with uniform noise in Type 1 for Example 1.**

Threshold	$\alpha$	0.1	0.3	0.5	0.7	1
	$h_x$					
50% noise	1/25	1.3898e-01	1.3898e-01	1.3898e-01	1.3898e-01	1.3898e-01
	1/50	8.1201e-02	8.1201e-02	8.1201e-02	8.1201e-02	8.1201e-02
	1/100	3.4951e-02	3.4951e-02	3.4951e-02	3.4951e-02	3.4951e-02
20% noise	1/25	1.4190e-01	1.4190e-01	1.4190e-01	1.4190e-01	1.4190e-01
	1/50	8.2515e-02	8.2515e-02	8.2515e-02	8.2515e-02	8.2515e-02
	1/100	1.6557e-02	1.6557e-02	1.6557e-02	1.6557e-02	1.6557e-02
10% noise	1/25	1.3998e-01	1.3998e-01	1.3998e-01	1.3998e-01	1.3998e-01
	1/50	8.1266e-02	8.1266e-02	8.1266e-02	8.1266e-02	8.1266e-02
	1/100	8.1891e-03	8.1891e-03	8.1891e-03	8.1891e-03	8.1891e-03
clean data	1/25	1.2192e-01	1.2192e-01	1.2192e-01	1.2192e-01	1.2192e-01
	1/50	8.1341e-02	8.1341e-02	8.1341e-02	8.1341e-02	8.1341e-02
	1/100	3.1629e-03	3.1629e-03	3.1629e-03	3.1629e-03	3.1629e-03

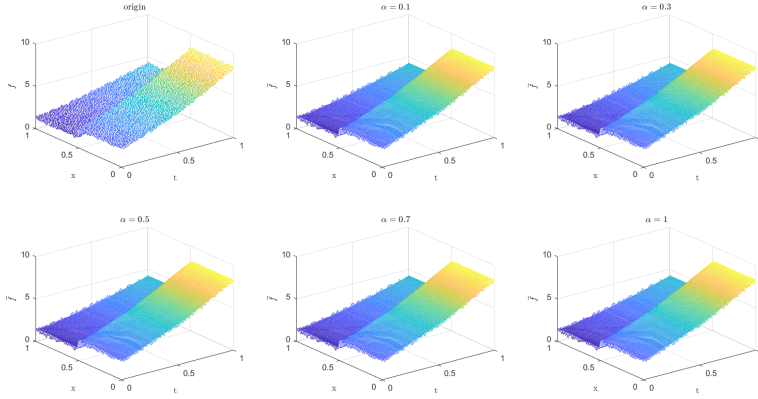


Fig. 4: **Discover  $\tilde{f}$  for  $h_x = h_t = 1/100$  with 50% uniform noise in Type 1 for Example 1.**



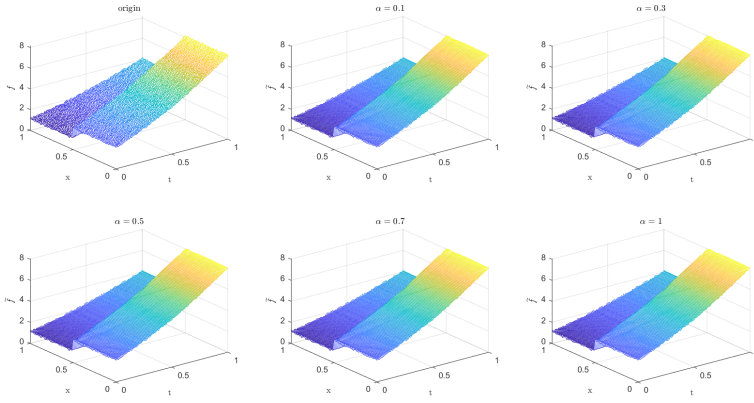


Fig. 5: Discover  $\tilde{f}$  for  $h_x = h_t = 1/100$  with 20% uniform noise in Type 1 for Example 1.

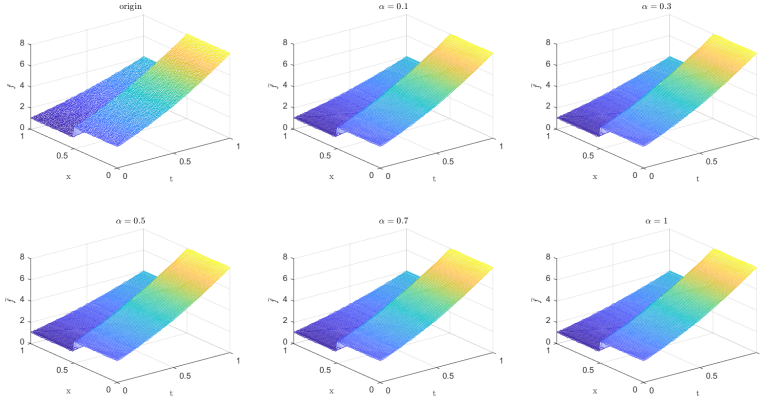


Fig. 6: Discover  $\tilde{f}$  for  $h_x = h_t = 1/100$  with 10% uniform noise in Type 1 for Example 1.

### 6.1.2 Type 2 in DNN

Table 2 and Figures 8-11 show the relative error (6.1) between the source function  $f$  in Example 1 and discovery  $\tilde{f}$  in (4.2) with epoch=250 in Type 2. The numerical experiments are given to illustrate the availability using deep learning. In fact, from Table 2, it can be found that our proposed algorithm is stable and accurate faced with different discretization sizes and noise level, and is also robust even for 50% uniformly distributed noise level.

*Example 2* Let us consider the following subdiffusion problem (1.1) with uniform noise

$$\begin{cases} {}_0^C D_t^\alpha u(x,t) - \Delta u = f, & x \in [0,1], t \in [0,1]; \\ u(x,0) = \sqrt{x(1-x)}; \\ u(0,t) = 0, u(1,t) = 0, \end{cases}$$

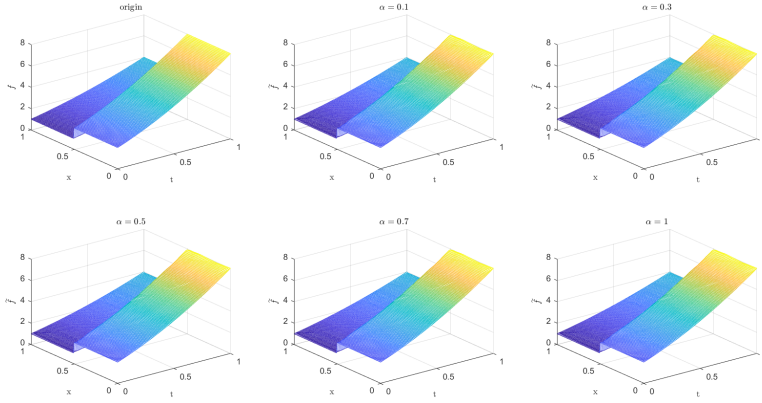


Fig. 7: Discover  $\tilde{f}$  for  $h_x = h_t = 1/100$  with clean data in Type 1 for Example 1.

Table 2: The relative error  $\|e_{\tilde{f}}\|_r$  with uniform noise in Type 2 for Example 1.

Threshold	$\alpha$					
	$h_x$	0.1	0.3	0.5	0.7	1
50% noise	1/25	1.0774e-01	1.0659e-01	1.0676e-01	1.0695e-01	1.0952e-01
	1/50	7.9438e-02	7.9069e-02	7.9516e-02	7.9440e-02	8.1030e-02
	1/100	5.2110e-02	5.1856e-02	5.1991e-02	5.2098e-02	5.2704e-02
20% noise	1/25	1.1791e-01	1.1925e-01	1.1919e-01	1.1859e-01	1.1716e-01
	1/50	7.9669e-02	8.0419e-02	8.0401e-02	7.9954e-02	7.9223e-02
	1/100	1.5546e-02	1.5030e-02	1.5171e-02	1.4991e-02	1.6229e-02
10% noise	1/25	1.2006e-01	1.2129e-01	1.2091e-01	1.2068e-01	1.2047e-01
	1/50	8.0694e-02	8.1230e-02	8.1086e-02	8.0716e-02	8.0783e-02
	1/100	1.0260e-02	9.6543e-03	9.5003e-03	9.5757e-03	1.0225e-02
clean data	1/25	1.2154e-01	1.2198e-01	1.2206e-01	1.2179e-01	1.2169e-01
	1/50	8.1152e-02	8.1369e-02	8.1410e-02	8.1255e-02	8.1141e-02
	1/100	4.8904e-03	3.7653e-03	3.7053e-03	3.6545e-03	4.7890e-03

where the source function with the random noise  $\delta$  is given by

$$f(x, t) = \begin{cases} (t+1)^{1/4} (1 + \chi_{(0,1/2)}(x)) + \delta, & 0 \leq x \leq 1/2; \\ (t+1)^2 (1 + \chi_{(0,1/2)}(x)) + \delta, & \text{otherwise.} \end{cases}$$

Here  $\delta$  is the uniform noise with 10% (clean data) 10%, 20%, 50% level for a single uniform distributed random number in the interval  $(0, 1)$ , respectively. In this experiment, we train the deep learning discovery  $\tilde{f}$  in (4.2).

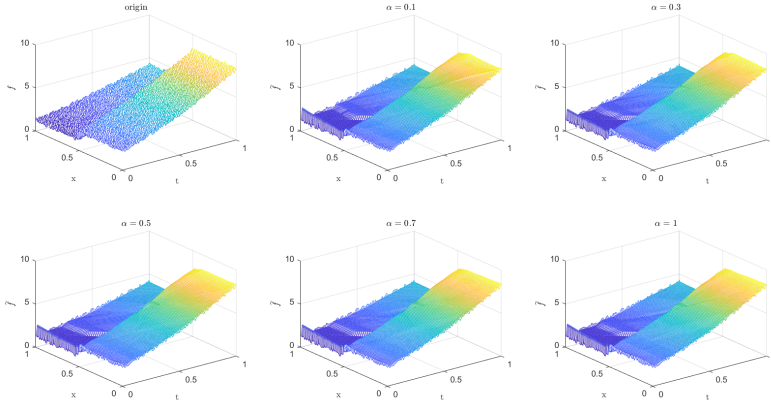


Fig. 8: Discover  $\tilde{f}$  for  $h_x = h_t = 1/100$  with 50% uniform noise in Type 2 for Example 1.

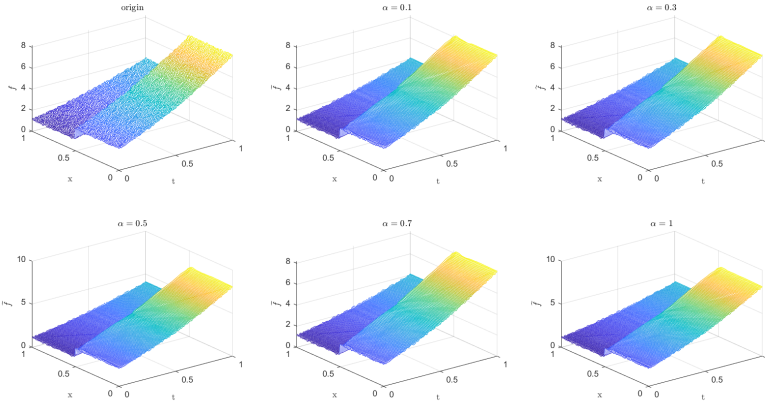


Fig. 9: Discover  $\tilde{f}$  for  $h_x = h_t = 1/100$  with 20% uniform noise in Type 2 for Example 1.

### 6.1.3 Type 1 in DNN

Table 3 and Figures 12-15 show the relative error (6.1) between the source function  $f$  in Example 2 and discovery  $\tilde{f}$  in (4.2) with different noise levels and epoch=200 in Type 1. The numerical experiments are given to illustrate the availability using deep learning for the different noise levels. From Table 3, it can be found that our proposed algorithm is stable and accurate faced with different discretization sizes and noise level, which is robust even for 50% uniformly distributed noise level. From Figures 12-15, it appears a layer or blows up at  $t = 0$  (boundary noise pollution), since the low time regularity [27, 28].

### 6.1.4 Type 2 in DNN

Table 4 and Figures 16-19 show the relative error (6.1) between the source function  $f$  in Example 1 and discovery  $\tilde{f}$  in (4.2) with different noise levels and epoch=270 in Type 2.

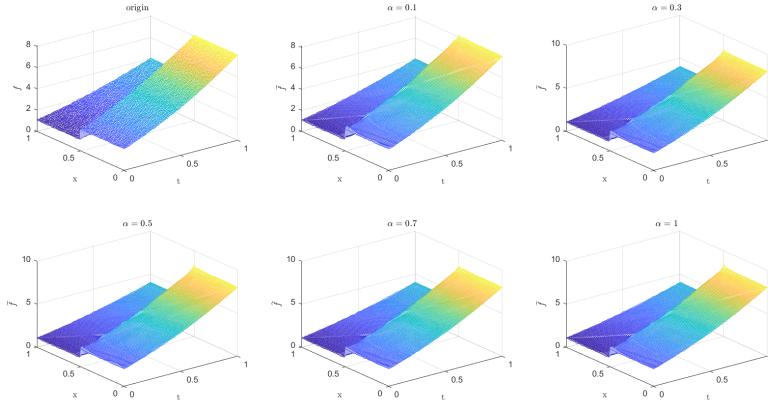


Fig. 10: Discover  $\tilde{f}$  for  $h_x = h_t = 1/100$  with 10% uniform noise in Type 2 for Example 1.

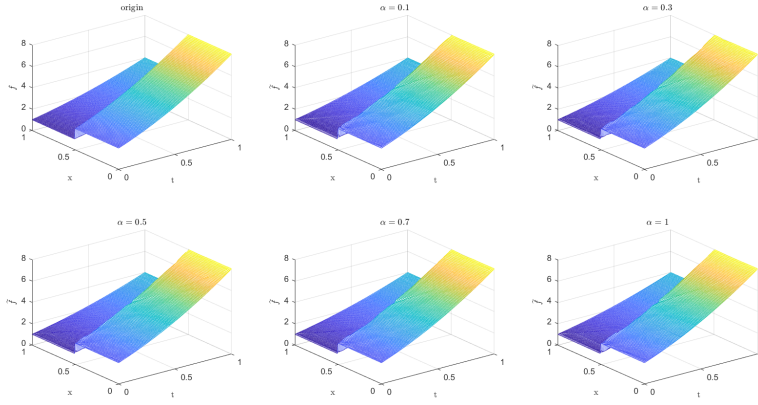
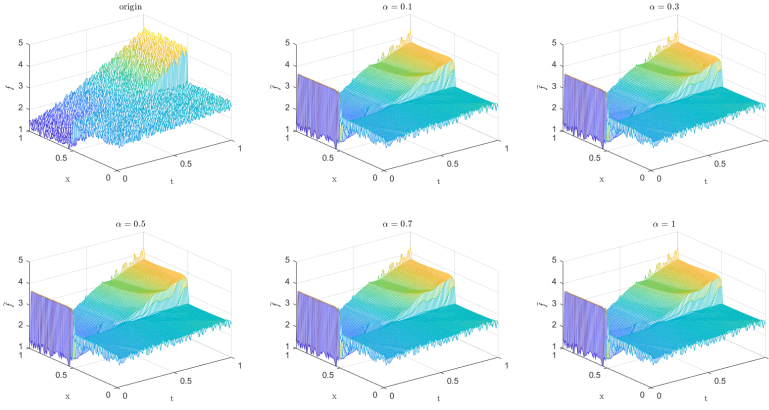


Fig. 11: Discover  $\tilde{f}$  for  $h_x = h_t = 1/100$  with clean data in Type 2 for Example 1.

The numerical experiments are given to illustrate the availability using deep learning for the different noise levels. From Table 4, it can be found that our proposed algorithm is stable and accurate faced with different discretization sizes and noise level, which is robust even for 50% uniformly distributed noise level. From Figures 16-19, it also appears a little layer or blows up at  $t = 0$  (boundary noise pollution), since the low time regularity [27,28]. It seems that Type 2 is better than Type1 from observed data.

Table 3: The relative error  $\|e_{\tilde{f}}\|_r$  with uniform noise in Type 1 for Example 2.

Noise Level	$\alpha$	0.1	0.3	0.5	0.7	1
	$h_x$					
50% noise	1/25	1.5132e-01	1.5132e-01	1.5132e-01	1.5132e-01	1.5132e-01
	1/50	1.2040e-01	1.2040e-01	1.2040e-01	1.2040e-01	1.2040e-01
	1/100	1.1607e-01	1.1607e-01	1.1607e-01	1.1607e-01	1.1607e-01
20% noise	1/25	1.1360e-01	1.1360e-01	1.1360e-01	1.1360e-01	1.1360e-01
	1/50	8.3587e-02	8.3587e-02	8.3587e-02	8.3587e-02	8.3587e-02
	1/100	6.1966e-02	6.1966e-02	6.1966e-02	6.1966e-02	6.1966e-02
10% noise	1/25	5.8198e-02	5.8198e-02	5.8198e-02	5.8198e-02	5.8198e-02
	1/50	4.2641e-02	4.2641e-02	4.2641e-02	4.2641e-02	4.2641e-02
	1/100	3.5011e-02	3.5011e-02	3.5011e-02	3.5011e-02	3.5011e-02
clean data	1/25	5.2867e-02	5.2867e-02	5.2867e-02	5.2867e-02	5.2867e-02
	1/50	3.7670e-02	3.7670e-02	3.7670e-02	3.7670e-02	3.7670e-02
	1/100	2.0318e-02	2.0318e-02	2.0318e-02	2.0318e-02	2.0318e-02

Fig. 12: Discover  $\tilde{f}$  for  $h_x = h_t = 1/100$  with 50% uniform noise in Type 1 for Example 2.

## 6.2 Numerical Experiments for discovery with Gaussian noise

*Example 3* Let us consider the Example 2 again with Gaussian noise, namely,

$$\begin{cases} {}_0^C D_t^\alpha u(x, t) - \Delta u = f, & x \in [0, 1], t \in [0, 1]; \\ u(x, 0) = \sqrt{x(1-x)}; \\ u(0, t) = 0, u(1, t) = 0, \end{cases}$$

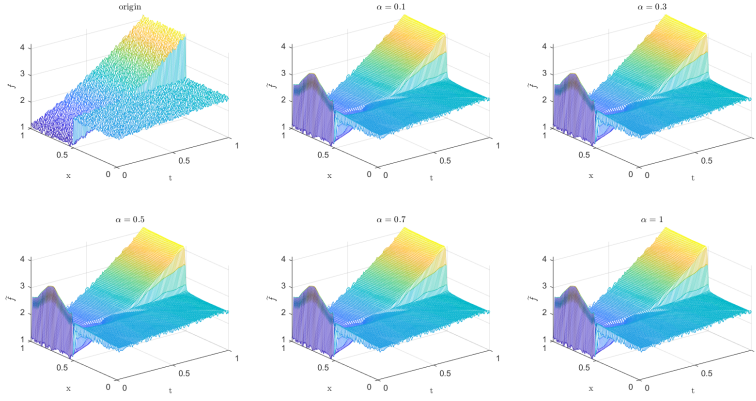


Fig. 13: Discover  $\tilde{f}$  for  $h_x = h_t = 1/100$  with 20% uniform noise in Type 1 for Example 2.

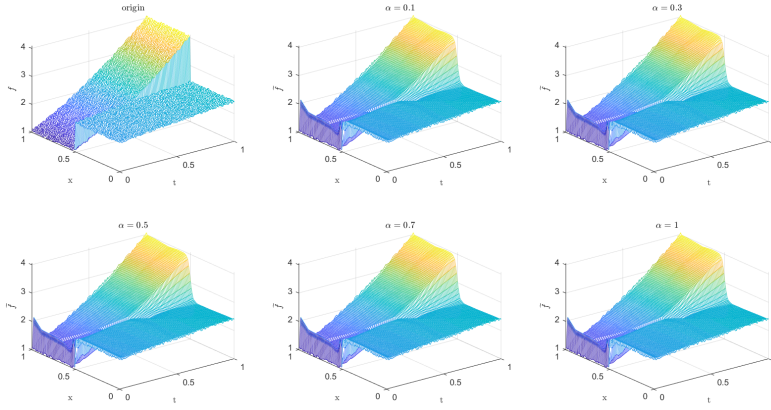


Fig. 14: Discover  $\tilde{f}$  for  $h_x = h_t = 1/100$  with 10% uniform noise in Type 1 for Example 2.

where the source function with the random noise  $\eta$  is given by

$$f(x, t) = \begin{cases} (t+1)^{1/4} (1 + \chi_{(0,1/2)}(x)) + \eta, & 0 \leq x \leq 1/2; \\ (t+1)^2 (1 + \chi_{(0,1/2)}(x)) + \eta, & \text{otherwise.} \end{cases}$$

Here  $\eta$  is the Gaussian noise with 10% (clean data) 10%, 20%, 50% level, respectively, which is statistical noise having a probability density function equal to that of the normal distribution. In this experiment, we train the deep learning discovery  $\tilde{f}$  in (4.2).

### 6.2.1 Type 1 in DNN

Table 5 and Figures 20-23 show the relative error (6.1) between the source function  $f$  in Example 2 and discovery  $\tilde{f}$  in (4.2) with different noise levels and epoch=255 in Type 1.

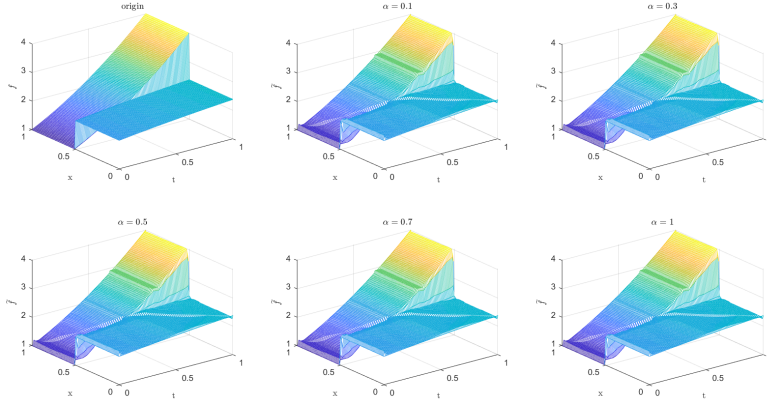


Fig. 15: Discover  $\tilde{f}$  for  $h_x = h_t = 1/100$  with clean data in Type 1 for Example 2.

Table 4: The relative error  $\|e_{\tilde{f}}\|_r$  with uniform noise in Type 2 for Example 2.

Noise Level	$\alpha$					
	$h_x$	0.1	0.3	0.5	0.7	1
50% noise	1/25	8.6685e-02	8.5475e-02	8.4797e-02	8.4731e-02	8.1521e-02
	1/50	7.2426e-02	7.1836e-02	7.1454e-02	7.1377e-02	6.9543e-02
	1/100	6.2809e-02	6.2084e-02	6.1725e-02	6.1470e-02	6.1917e-02
20% noise	1/25	6.6977e-02	6.7135e-02	6.6908e-02	6.7067e-02	6.7562e-02
	1/50	4.8547e-02	4.8697e-02	4.8523e-02	4.8578e-02	4.8868e-02
	1/100	2.7690e-02	2.7786e-02	2.7643e-02	2.7814e-02	2.7819e-02
10% noise	1/25	6.3849e-02	6.3655e-02	6.3809e-02	6.3935e-02	6.3953e-02
	1/50	4.3969e-02	4.3909e-02	4.3996e-02	4.4066e-02	4.4010e-02
	1/100	1.8282e-02	1.8648e-02	1.8545e-02	1.8526e-02	1.8353e-02
clean data	1/25	5.6927e-02	5.8353e-02	5.8272e-02	5.7993e-02	5.8502e-02
	1/50	3.8296e-02	3.9283e-02	3.9420e-02	3.9318e-02	3.9337e-02
	1/100	5.4745e-03	4.4494e-03	4.9254e-03	4.7000e-03	3.9269e-03

The numerical experiments are given to illustrate the availability using deep learning for the different noise levels. From Table 5, it can be found that our proposed algorithm is stable and accurate faced with different discretization sizes and noise level, which is robust even for 50% Gaussian noise level. From Figures 20-23, it also appears a layer or blows up at  $t = 0$  (boundary noise pollution).

### 6.2.2 Type 2 in DNN

Table 6 and Figures 24-26 show the relative error (6.1) between the source function  $f$  in Example 2 and discovery  $\tilde{f}$  in (4.2) with different noise levels and epoch=270 in Type 2. The numerical experiments are given to illustrate the availability using deep learning for the

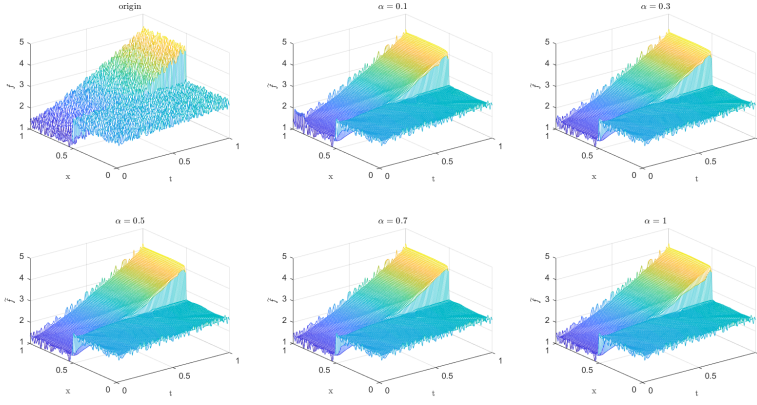


Fig. 16: Discover  $\tilde{f}$  for  $h_x = h_t = 1/100$  with 50% uniform noise in Type 2 for Example 2.

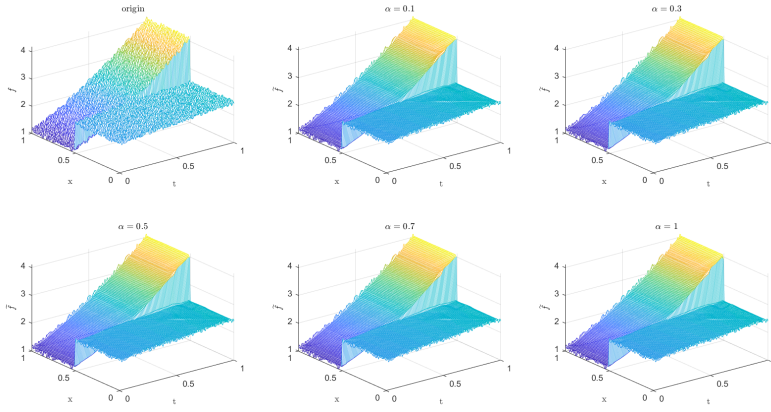


Fig. 17: Discover  $\tilde{f}$  for  $h_x = h_t = 1/100$  with 20% uniform noise in Type 2 for Example 2.

different noise levels. From Table 6, it can be found that our proposed algorithm is stable and accurate faced with different discretization sizes and noise level, which is robust even for 50% Gaussian noise level. From Figures 24-26, it also appears a little layer or blows up at  $t = 0$  (boundary noise pollution).

## 7 Conclusion

In this work, we firstly propose the discovery of subdiffusion with noisy data in deep learning based on the designing two types. The numerical experiments are given to illustrate the availability using deep learning even for the 50% noise level. The advantage of first Type is that model (4.2) can be trained for each fixed  $\alpha$ , which reduces the computational count and



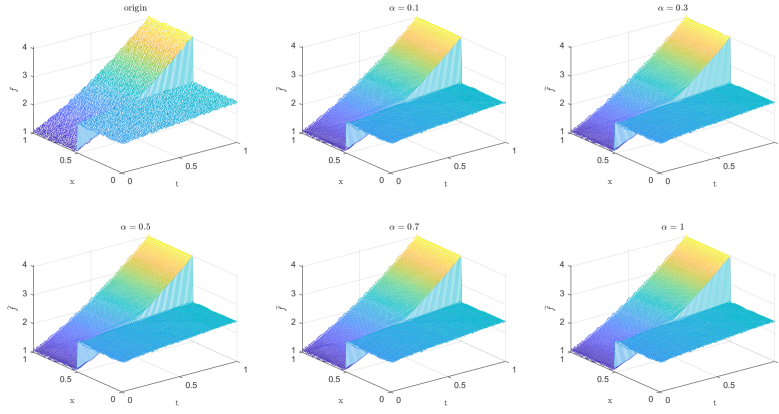


Fig. 18: Discover  $\tilde{f}$  for  $h_x = h_t = 1/100$  with 10% uniform noise in Type 2 for Example 2.

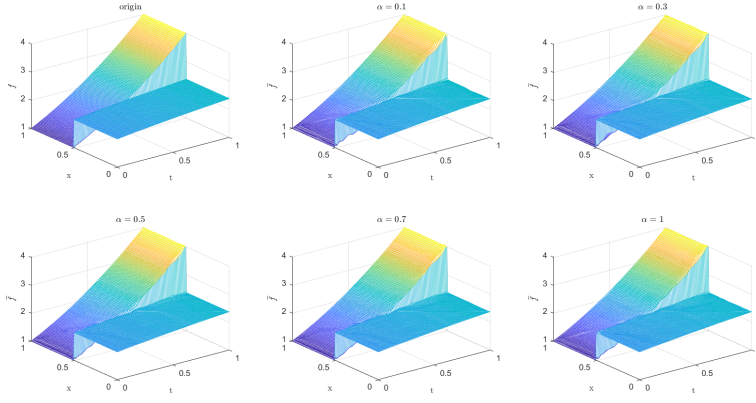
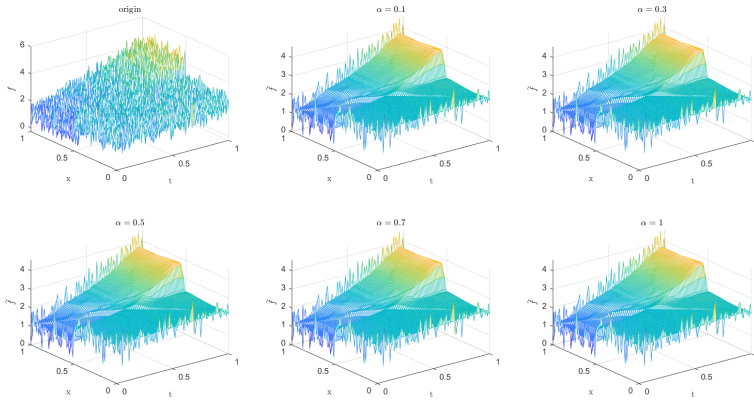


Fig. 19: Discover  $\tilde{f}$  for  $h_x = h_t = 1/100$  with clean data in Type 2 for Example 2.

required storage, since it fixes  $\alpha$  as input data. Obviously, it may loss some accuracy. To recover the accuracy, second Type is complemented, which needs more computational count. It implies an interesting generalized structure by combining Type 1 and Type 2, which may keep suitable accuracy and reduces computational count. As a result, even when discovering the interger-order equations, the proposed type DNNs have some advantages compared with the traditional numerical scheme and previous works to solve the data-driven discovery for differential equations. The interesting topic is reducing the computational count and storage by fast multigrid or conjugate gradient squared method [1,4]. Another interesting topic is how to design the correction of  $L_1$  approximation for reducing the boundary noise pollution, since subdiffusion model appears a layer or blows up at  $t = 0$  [27,28] with low time regularity.

Table 5: The relative error  $\|e_{\tilde{f}}\|_r$  with Gaussian noise in Type 2 for Example 3.

Threshold	$\alpha$	0.1	0.3	0.5	0.7	1
	$h_x$					
50% noise	1/25	2.1181e-01	2.1181e-01	2.1181e-01	2.1181e-01	2.1181E-01
	1/50	2.1048e-01	2.1048e-01	2.1048e-01	2.1048e-01	2.1048e-01
	1/100	2.1618e-01	2.1618e-01	2.1618e-01	2.1618e-01	2.1618e-01
20% noise	1/25	1.1250e-01	1.1250e-01	1.1250e-01	1.1250e-01	1.1250e-01
	1/50	9.5174e-02	9.5174e-02	9.5174e-02	9.5174e-02	9.5174e-02
	1/100	9.1433e-02	9.1433e-02	9.1433e-02	9.1433e-02	9.1433e-02
10% noise	1/25	1.1917e-01	1.1917e-01	1.1917e-01	1.1917e-01	1.1917e-01
	1/50	8.6597e-02	8.6597e-02	8.6597e-02	8.6597e-02	8.6597e-02
	1/100	7.4511e-02	7.4511e-02	7.4511e-02	7.4511e-02	7.4511e-02
clean data	1/25	7.0042e-02	7.0042e-02	7.0042e-02	7.0042e-02	7.0042e-02
	1/50	4.0945e-02	4.0945e-02	4.0945e-02	4.0945e-02	4.0945e-02
	1/100	1.4316e-02	1.4316e-02	1.4316e-02	1.4316e-02	1.4316e-02

Fig. 20: Discover  $\tilde{f}$  for  $h_x = h_t = 1/100$  with 50% Gaussian noise in Type 1 for Example 3.

## References

1. Cao, R.J., Chen, M.H., Ng, M.K., Wu, Y.J.: Fast and high-order accuracy numerical methods for time-dependent nonlocal problems in  $\mathbb{R}^2$ . *J. Sci. Comput.* **84:8** (2020).
2. Chen, J.R., Jin, S., Lyu, L.Y.: A Deep learning Based Discontinuous Galerkin Method for Hyperbolic Equations with Discontinuous Solutions and Random Uncertainties. arXiv:2107.01127
3. Chen, M.H., Jiang, S.Zh., Bu, W.P.: Two  $L1$  schemes on graded meshes for fractional Feynman-Kac equation. *J. Sci. Comput.* **88:58** (2021)
4. Chen, M.H., Ekström, S.E., Serra-Capizzano, S.: A Multigrid method for nonlocal problems: non-diagonally dominant or Toeplitz-plus-tridiagonal systems. *SIAM J. Matrix Anal. Appl.* **41** 1546-1570 (2020)

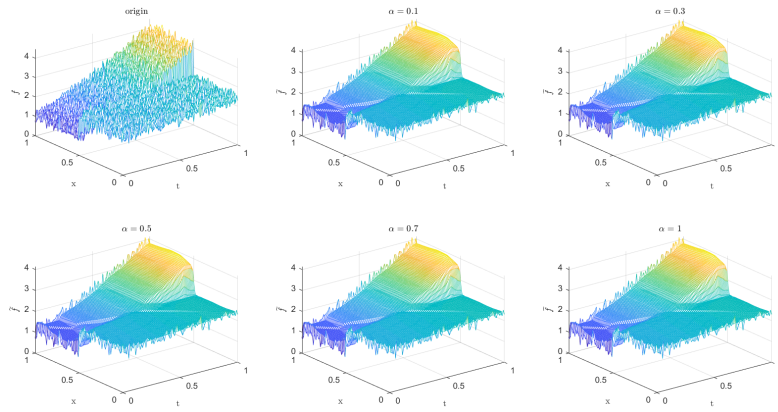


Fig. 21: Discover  $\tilde{f}$  for  $h_x = h_t = 1/100$  with 20% Gaussian noise in Type 1 for Example 3.

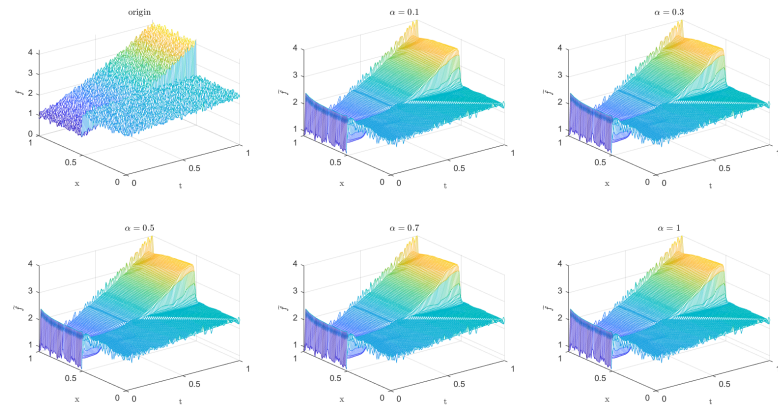


Fig. 22: Discover  $\tilde{f}$  for  $h_x = h_t = 1/100$  with 10% Gaussian noise in Type 1 for Example 3.

5. Chen, W.Q., Wang, Q., Hesthaven, J.S., Zhang, C.H.: Physics-informed machine learning for reduced-order modeling of nonlinear problems. *J. Comput. Phys.* **446**, 110666 (2021)
6. Eliazar, I., Klafter, J.: Anomalous is ubiquitous. *Ann. Physics* **326**, 2517–2531 (2011)
7. Du, Q., Gu, Y.Q., Yang, H.Z., Zhou, C.: The discovery of dynamics via linear multistep methods and deep learning:error estimation. arXiv:2103.11488
8. Duan, C.G., Jiao, Y.L., Lai, Y.M., Lu, X.L., Yang, Z.J.: Convergence rate analysis for deep Ritz method. arXiv:2103.13330
9. E, W.N., Yu, B.: The Deep Ritz method:A deep learning-based numerical algorithm for solving variational problems. *Commun. Math. Stat.* **6**, 1–12 (2018)
10. Goodfellow, I., Bengio, Y., Courville, A.: *Deep Learning*. Adaptive Computation and Machine Learning. MIT Press, Cambridge (2016)
11. Gu, Y.Q., Ng, M.K.: Deep Ritz method for the spectral fractional Laplacian equation using the Caffarelli-Silvestre extension. arXiv:2108.11592
12. Gulian, M.K., Raissi, M., Perdikaris, P., Karniadakis, G.: Machine learning of space-fractional differential equations. *SIAM J. Sci. Comput.* **41**, A2485–A2509 (2019)
13. Jiao, Y.L., Lai, Y.M., Lo, Y.S., Wang, Y., Yang, Y.F.: Error Analysis of Deep Ritz Methods for Elliptic Equations. arXiv:2107.14478

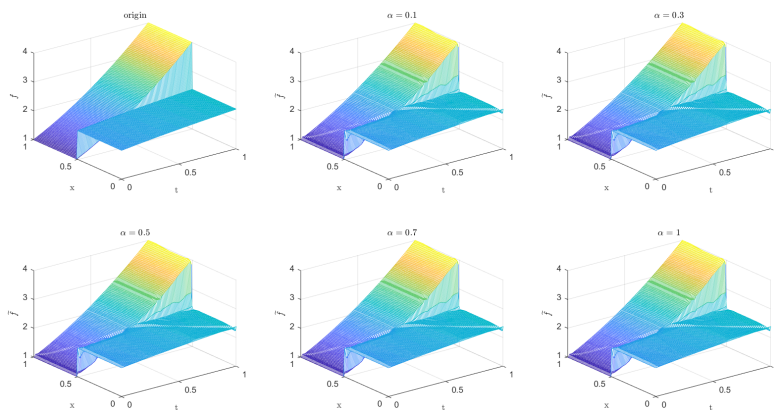


Fig. 23: Discover  $\tilde{f}$  for  $h_x = h_t = 1/100$  with clean data in Type 1 for Example 3.

Table 6: The relative error  $\|e_{\tilde{f}}\|_r$  with Gaussian noise in Type 2 for Example 3.

Threshold	$\alpha$					
	$h_x$	0.1	0.3	0.5	0.7	1
$h_x^* = h_t^*$ = 1/100 with 50% noise	1/25	2.1509e-01	2.1435e-01	2.1464e-01	2.1482e-01	2.1413e-01
	1/50	2.1005e-01	2.0957e-01	2.0972e-01	2.0975e-01	2.0946e-01
	1/100	2.0500e-01	2.0510e-01	2.0529e-01	2.0529e-01	2.0537e-01
$h_x^* = h_t^*$ = 1/100 with 20% noise	1/25	1.0418e-01	1.0426e-01	1.0441e-01	1.0465e-01	1.0478e-01
	1/50	9.2908e-02	9.2833e-02	9.2892e-02	9.3044e-02	9.2955e-02
	1/100	8.5171e-02	8.4946e-02	8.5225e-02	8.5757e-02	8.8259e-02
$h_x^* = h_t^*$ = 1/100 with 10% noise	1/25	7.3662e-02	7.4271e-02	7.4214e-02	7.4147e-02	7.4018e-02
	1/50	5.7890e-02	5.8266e-02	5.8156e-02	5.8111e-02	5.8036e-02
	1/100	4.2822e-02	4.2814e-02	4.2745e-02	4.2785e-02	4.2809e-02
$h_x^* = h_t^*$ = 1/100 with 0% noise	1/25	5.6927e-02	5.8353e-02	5.8272e-02	5.7993e-02	5.8502e-02
	1/50	3.8296e-02	3.9283e-02	3.9420e-02	3.9318e-02	3.9337e-02
	1/100	5.4745e-03	4.4494e-03	4.9254e-03	4.7000e-03	3.9269e-03

14. Keller, R., Du, Q.: Discovery of dynamics using linear multistep methods. SIAM J. Numer. Anal. **59**, 429–455 (2021)
15. Li, Y.J., Wang, Y.J., Deng, W.H.: Galerkin finite element approximations for stochastic space-time fractional wave equations. SIAM J. Numer. Anal. **55**, 3173–3202 (2017)
16. Li, Z.Y., Kovachki, N., Azzizadenesheli, K., Liu, B., Bhattacharya, K., Stuart, A., Anandkumar, A.: Markov Neural Operators for Learning Chaotic Systems. arXiv:2106.06898
17. Lin, Y.M., Xu, C.J.: Finite difference/spectral approximations for the time-fractional diffusion equation. J. Comput. Phys. **225**, 1533–1552 (2007)
18. Meerschaert, M.M., Sikorskii, A.: Stochastic Models for Fractional Calculus. de Gruyter GmbH Berlin (2012)
19. Metzler R., Klafter J.: The random walk's guide to anomalous diffusion: a fractional dynamics approach. Phys. Rep. **339**, 1–77 (2000)
20. Podlubny I.: Fractional Differential Equations. Academic Press, New York (1999)

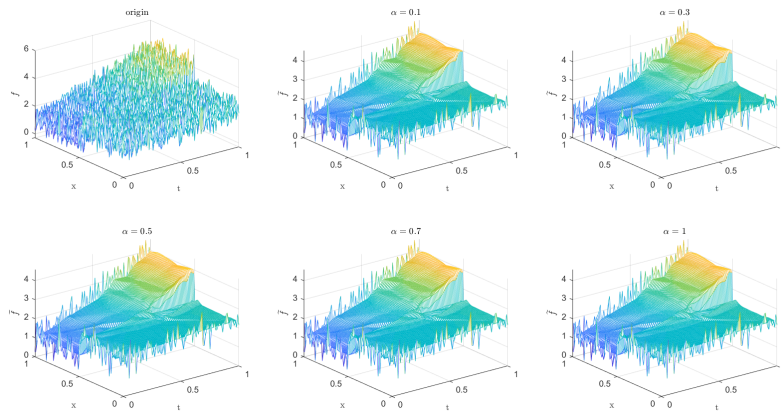


Fig. 24: Discover  $\tilde{f}$  for  $h_x = h_t = 1/100$  with 50% Gaussian noise in Type 2 for Example 3.

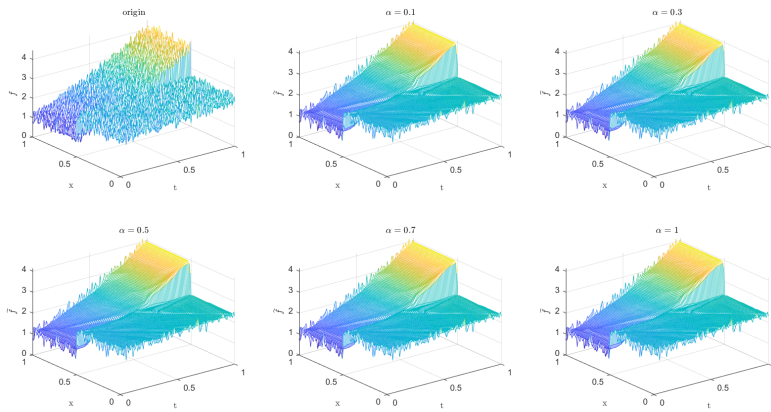


Fig. 25: Discover  $\tilde{f}$  for  $h_x = h_t = 1/100$  with 20% Gaussian noise in Type 2 for Example 3.

21. Qin, T., Wu, K., Xiu, D.: Data driven governing equations approximation using deep neural network. *J. Comput. Phys.* **395**, 620–635 (2019)
22. Raissi, M.: Deep hidden physics models deep learning of nonlinear partial differential equations. *The Journal of Machine Learning Research.* **19**, 1–24 (2018)
23. Rudy, S.H., Kutz, J.N., Brunton, S.L.: Deep learning of dynamics and signal-noise decomposition with time-stepping constraints. *J. Comput. Phys.* **396**, 483–506 (2019)
24. Shen, Z.W., Yang, H.Z., Zhang, S.J.: Deep Network Approximation Characterized by Number of Neurons *Commun. Comput. Phys.*, **28**, 1768–1811 (2019)
25. Shen, X., Cheng, X.L., Liang, .K.W.: Deep Euler Method: Solving ODEs by approximating the local truncation error of the euler method. arXiv:2003.09573
26. Sirignano, J., Spiliopoulos, K.: DGM: A deep learning algorithm for solving partial differential equations. *J. Comput. Phys.* **375**, 1339–1364 (2018)
27. Shi, J.K., Chen, M.H.: Correction of high-order BDF convolution quadrature for fractional Feynman-Kac equation with Lévy flight. *J. Sci. Comput.* **85:28** (2020)
28. Stynes, M., O’riordan, E., Gracia, J.L.: Error analysis of a finite difference method on graded meshes for a time-fractional diffusion equation. *SIAM J. Numer. Anal.* **55**, 1057–1079 (2017)

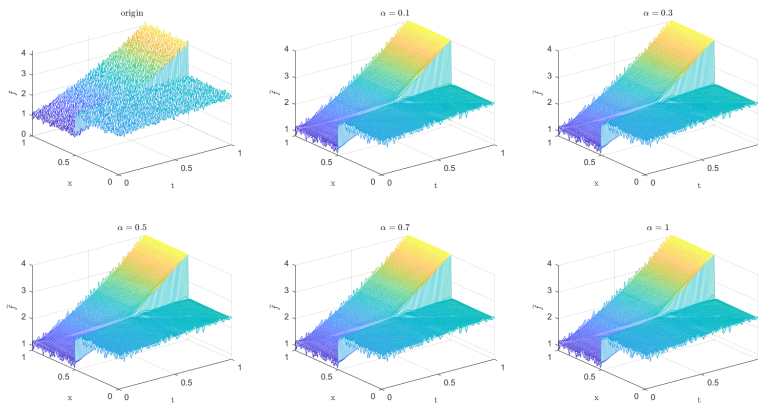


Fig. 26: Discover  $\hat{f}$  for  $h_x = h_t = 1/100$  with clean data in Type 2 for Example 3.

29. Tipireddy, R., Perdikaris, P., Stinis, P., Tartakovsky, A.: A comparative study of physics-informed neural network models for learning unknown dynamics and constitutive relations. arXiv:1904.04058
30. Wang, C., Chen, M.H., Deng, W.H., Bu, W.P., Dai, X.J.: A sharp error estimate of Euler–Maruyama method for stochastic Volterra integral equations. Math. Method Appl. Sci. Minor Revised.
31. Xu, Y., Zhang, H., Li, Y.G., Zhou, K., Liu, Q., Jurgen, K.: Solving Fokker-Planck equation using deep learning. Chaos. **30**, 013133 (2020)
32. Zhang, Z.H., Karniadakis, G.E.: Numerical Methods for Stochastic Partial Differential Equations with White Noise. Springer, New York (2017)